



EUROfusion

EUROFUSION WPD TT2-CP(16) 15137

F Crisanti et al.

DTT: an Integrated Bulk and Edge Plasma Experiment to Tackle the Power Exhaust Problem in View of DEMO

Preprint of Paper to be submitted for publication in
Proceedings of 26th IAEA Fusion Energy Conference



This work has been carried out within the framework of the EUROfusion Consortium and has received funding from the Euratom research and training programme 2014-2018 under grant agreement No 633053. The views and opinions expressed herein do not necessarily reflect those of the European Commission.

This document is intended for publication in the open literature. It is made available on the clear understanding that it may not be further circulated and extracts or references may not be published prior to publication of the original when applicable, or without the consent of the Publications Officer, EUROfusion Programme Management Unit, Culham Science Centre, Abingdon, Oxon, OX14 3DB, UK or e-mail Publications.Officer@euro-fusion.org

Enquiries about Copyright and reproduction should be addressed to the Publications Officer, EUROfusion Programme Management Unit, Culham Science Centre, Abingdon, Oxon, OX14 3DB, UK or e-mail Publications.Officer@euro-fusion.org

The contents of this preprint and all other EUROfusion Preprints, Reports and Conference Papers are available to view online free at <http://www.euro-fusionscipub.org>. This site has full search facilities and e-mail alert options. In the JET specific papers the diagrams contained within the PDFs on this site are hyperlinked

DTT: an Integrated Bulk and Edge Plasma Experiment to Tackle the Power Exhaust Problem in View of DEMO

F. Crisanti¹, R. Albanese², R. Ambrosino², G. Calabrò¹, S. Minucci², R. Lombroni³ and V. Pericoli Ridolfini²

¹ENEA, Dipartimento FSN, C. R. Frascati, via E. Fermi 45, 00044 Frascati (Roma), Italy

²Consorzio CREATE, Università di Napoli Federico II, Via Claudio 21, 80125 Napoli, Italy

⁴School of Engineering – DEIM, University of Tuscia, Largo dell'Università snc, 01100 Viterbo, Italy

E-mail contact of main author: flavio.crisanti@enea.it


Abstract. This paper explores the heat load reduction capabilities of using a set of internal poloidal field coils, capable to locally modify the magnetic field in the vicinity of the divertor target, for a dedicated Divertor Tokamak Test (DTT) facility. Objectives, figure of merits and specifications considered in the design of the DTT equilibrium configurations will be firstly illustrated. The range of alternative plasma shapes the potential heat flux mitigation effects are then discussed. Finally edge plasma transport simulations will be presented.

1. Introduction

Within the frame of the DTT program, included in the EuroFusion roadmap [1], the design of a new Tokamak dedicated to tackle the Power Exhaust problem as an integrated bulk and edge plasma problem has been recently developed [2]. The main objective of the Divertor Tokamak Test (DTT) facility is to host experiments addressed to the solution of the power exhaust issues in view of DEMO. This derives from the need to develop integrated and controllable exhaust solutions including Plasma Facing Components (PFCs), control diagnostics and actuators, using experiments, theory and modelling, so as to mitigate the risk that conventional divertor might not be suitable for DEMO [3]. The requirements are detailed in [2, 3], and include: specifications on a number of normalized plasma parameters relevant for DEMO; ratio between power crossing the separatrix P_{sep} and the major radius R relevant for DEMO ($P_{sep}/R \geq 15$ MW/m); flexibility in the divertor region so as to possibly test different divertors; possibility to test alternative magnetic configurations; possibility to test liquid metals; integrated scenarios (solutions to be compatible with plasma performance and technological constraints of DEMO); budget constraint of 500 M€. These requirements led to the selection of the following parameters: a major radius of $R=2.15$ m, a minor radius $a=0.7$ m, an aspect ratio of about $R/a \approx 3$, an elongation of $\kappa \approx 1.7$, a triangularity of $\delta \approx 0.35$, a toroidal field of $B_T=6$ T, a plasma current of $I_p=6$ MA, and a flat top of about 100 s [2, 3][3]. Promising experimental results on alternative configurations have been obtained in DIII-D [4], EAST [5], NSTX [6], TCV [7] and planned to be executed on MAST-U [8]. The DTT device will addresses the challenge of investigate alternative magnetic configurations including snowflake [9, 10], quasi-snowflake [5] and X-divertor [11] equilibria with plasma conditions similar to DEMO. Here, the potential benefits of using in-vessel poloidal field coils, to locally modify the magnetic configuration in the divertor region with currents ≤ 60 kAt, will be discussed in details.

The paper is organized as follows. Section 2 describes how the installation of a set of in-vessel PF coils enables a variety of divertor geometries. Section 3 identifies a series of potential heat flux mitigation effects that could be investigated. Section 4 presents predictive edge simulations using the TECXY numerical code by comparing an alternative configuration with the reference single null. Finally, the main conclusions will be given.

2. In-vessel poloidal field coils and advanced equilibrium configurations

The study of the divertor physics and technology is one of the main target  the DTT. Indeed, for optimizing the local magnetic configuration and consequently controlling various parameters related to the power exhaust (flux expansion, connection length, distance between null points, etc.), DTT will be equipped with a set of internal coils capable to locally modify the magnetic field in the vicinity of the divertor target. Using these in-vessel coils, it will be possible to adjust a second null region in Snowflake-like configurations [5, 9, 10], obtaining a large area where the poloidal magnetic field B_p and its gradient are close to zero or defining XD-like configuration where the flux flaring at target can be largely varied.

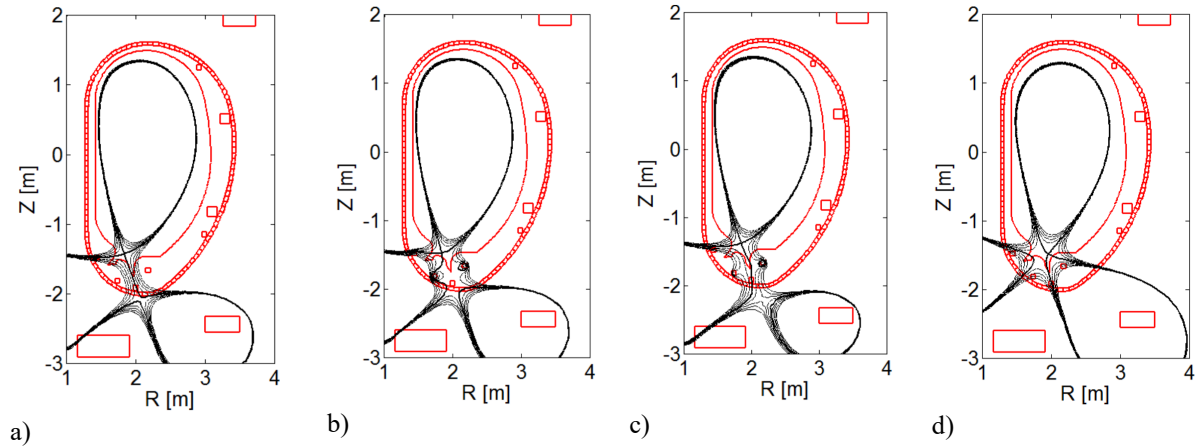


Figure 1. a) SF^+ equilibrium with no current flowing in the in-vessel coils; b) SF^- equilibrium generated from the reference SF^+ with the use of the internal coils: $C1 = 28.7kA$, $C2 = -60kA$, $C3 = 0.5kA$, $C4 = 50.7kA$ coils; c) X-d like equilibrium generated from the reference SF^+ with the use of the internal coils; d) SF equilibrium with no current flowing in the in-vessel coils.

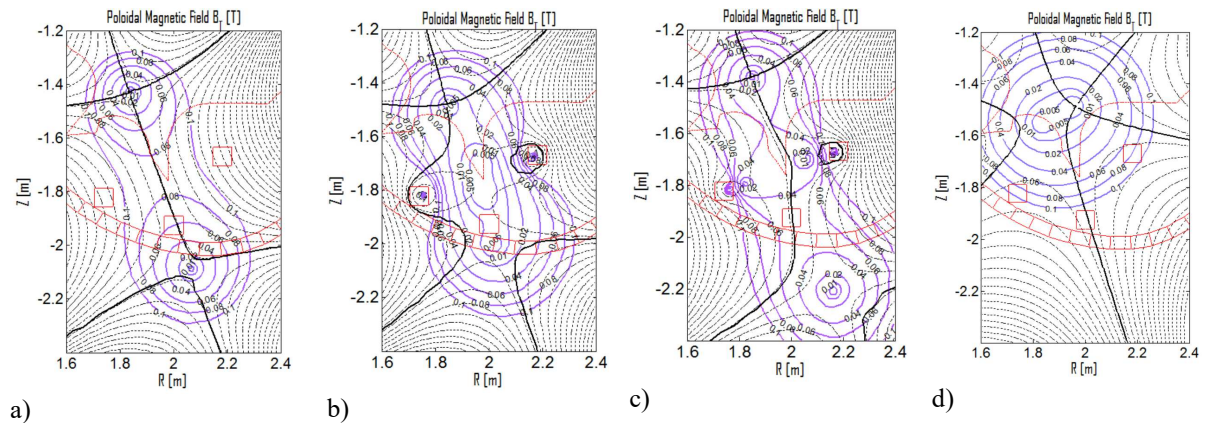


Figure 2. a) poloidal magnetic field B_p of the SF^+ configuration in the divertor region $[0-0.1T]$; b) poloidal magnetic field B_p of the SF^- configuration in the divertor region $[0-0.1T]$; c) poloidal magnetic field B_p of the SF^- configuration in the divertor region $[0-0.1T]$; d) poloidal magnetic field B_p of the SF^+ configuration in the divertor region $[0-0.1T]$.

As example of the flexibility of a such system, the SF^+ equilibrium, with $I_p=5MA$, discussed in details in [12] and shown in Fig. 1a), has been considered as starting point in our analysis with no current flowing in the internal coils, anti-clockwise labelled C1-C4. An advanced SF^- like configuration can be obtained by using the in-vessel coils, as shown in Fig. 1b), modifying the distance and the poloidal flux difference between the two nulls from SF^+ (Fig. 2a) to SF^- (Fig. 2b) and consequently modifying the flux flaring around the main null, characterized by the magnetic field gradient. Indeed, the dependence of ∇B_p (the gradient of the poloidal magnetic field B_p) ~~in the primary x-point~~ on the distance between nulls is described in [12] as criterion of interdependence between them. A self-explanatory way to show the aforementioned dependence is to plot the iso-contours of B_p around the nulls, as discussed in [5, 13], for the SF configurations with and without in-vessel coils (Figs. 2a and 2b). A direct manifestation of the interdependence between the nulls is that the flux flaring (characterized by the poloidal field gradient) in the main null is affected by the presence of the second null. As shown in Figs. 2) a-d, ∇B_p depends on the distance between the nulls. This flaring is then directly translated to an increase of the main magnetic divertor geometry parameters (as poloidal flux expansion and connection length [9, 10, 13], evaluated for the flux surface at 2 mm from the boundary and starting from the mid-plane up to the target), as reported in Table I, and consequently, to an increased wetted surface area and reduced heat flux [5, 9, 10, 13].

TABLE I
COMPARISON OF FLUX EXPANSION AND CONNECTION LENGTH OF THE SF CONFIGURATIONS
WITH AND WITHOUT INTERNAL COILS WITH CALCULATED WITH A SCRAPE-OFF (SOL) DECAY LENGTH $\lambda_q=2MM$

	Flux expansion IN Target/ X-point	Flux expansion OUT Target/ X-point	Connection Length IN	Connection Length OUT
SN, no in-vessel coils: C1-C4 = 0kA	11.84/53.53	10.86/47.27	42.64	23.64
SF+, no in-vessel coils: C1-C4 = 0kA	20.49/94.55	29.29/73.41	57.91	42.73
SF-, in-vessel coils: C1 = 28.7kA, C2 = -60kA, C3 = 0.5kA, C4 = 50.7kA	22.74/256.68	75.73/91.33	58.36	67.75
X-d, in-vessel coils: C1 = -2,5kA, C2 = -43kA, C3 = -0.5kA, C4 = 50.7kA	20.08/95.17	40.83/71.67	70.36	51.49
SF, no in-vessel coils: C1-C4 = 0kA	??	28.87/96.20	96.67	45.58

Table I includes also the data for the standard Snowflake (SF), shown in Fig. 1d and Fig. 2d, and Single Null (SN), not shown here and discussed in [2, 3], obtained without in-vessel coils. It should be noted that the SF equilibrium has been calculated at lower $I_p=4MA$, and consequently, presents a lower outer connection length (L_c) with respect at SF^- reported in Table I. A detailed discussion of the potential heat flux mitigation effects related to the geometry parameters, described in Table I, will be presented in next Section. In addition, a X-d like configuration could be further studied by means of in-vessel coils as shown in Fig. 1c and Fig. 2c, focusing on the possibility to creating a third null in the proximity of the outer target. The installation of a pair of PF coils with currents ≤ 60 kA enables a further variety of

divertor geometries, not discussed here. The current saturation at 60 kA might limit the performance of the in-vessel coil system. However, there is the possibility of doubling the cross section of each internal turn, which is feasible according to the thermal analysis reported in [2], or reducing the reference plasma current of the configuration.

3. Potential heat flux mitigation effects

All the divertor magnetic alternative configurations show the feature to potentially increase the divertor target flux expansion, spreading out the power flux on a larger surface [4-13]; but straightforward algebraic evaluations can easily show that this geometrical effect is not sufficient, on a future fusion reactor, to reduce the plates power flux density down to the safe value $P_{\text{Plates}} < 10 \text{ MW/m}^2$, compatible with the present material available technology. Consequently, it becomes crucial an “integration” of the alternative magnetic configuration

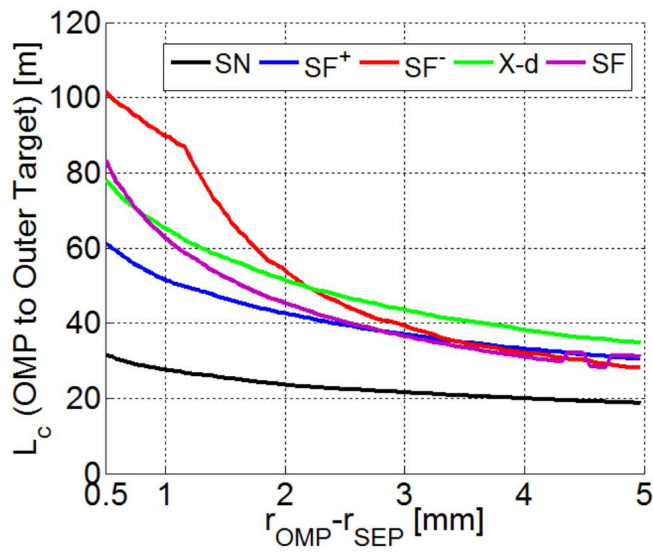


FIG. 3. Connection length (L_c) from outer midplane (OMP) to outer target along the Scrape-Off layer (SOL).

could constrain the cold radiative region close to the second null, i.e. just in front of the divertor plates [13]. The importance of the synergy between the local radiation and the magnetic configuration connected with the completed ignorance regarding the most important involved physics mechanism are at the basis of designing a very machine capable to play with the reciprocal position of the nulls ranging between the two extreme cases of the SF and X-d, but including “intermediate” situations where such a pure distinction is not any more possible, but able to address the role played the local magnetic topology. The four equilibria (SF⁺ SF⁻, X-d, SF) illustrated in the previous section are, in same way, trying to represent what we have just discussed. As first rough evaluation we can compare the flux expansions and the connection lengths on both outer target and main X-point region (Table 1). The flux expansion is always larger than the one of the SN, but if the enhancement at the X-point is more or less the same for all of them, the situation changes at the target; here, as expected, the gain is larger for the X-d (up to a factor ≈ 4) than for the two SF like configuration ($\text{SF} \approx \text{SF}^+ \approx 2.5$). The situation slightly changes for the SF⁻ characterized by the fact that the two nulls are strictly linked, i.e. among the two nulls there is a region with a very low poloidal field (Fig. 2b). Obviously also the connection length increases for all the configurations of a factor ≈ 2 -3, where again the SF⁻ configuration shows the larger gain. As discussed in [14], a longer connection length means that a particle dwells longer in the edge region, with a

with the local losses of energy (radiation by atomic transition: directs or impurities; momentum losses: radiation by bremsstrahlung,...). In this respect we can expect a large difference among the different magnetic geometries, having as two extreme cases the standard SF and an X-d configuration. In the first case the large region with very low poloidal field can be the driving source for large convective fluxes [12], with a consequent large radiation loss localized in the field null region; on the contrary the “hilly” behaviour of the poloidal field flux between the two “small” regions of null field

subsequent strong enhancement of the radiative losses. From these first rough evaluation it should be expected that the stronger synergy between the magnetic configuration and the radiative processes it should be expected for the SF⁻ configuration, followed by the X-d; the other two configurations, although, always much better than the SN, should give less advantage. This looking only at “classical” effects; the situation could be very different if local convection (or turbulence) is the dominant physics. In this case the situation could be reversed and the two SF configurations being the ones the stronger radiative synergy. In Fig. 3 the connection lengths of the all the configuration are reported versus a figure of the flux surface (i.e. the distance on mid-plane from the boundary).

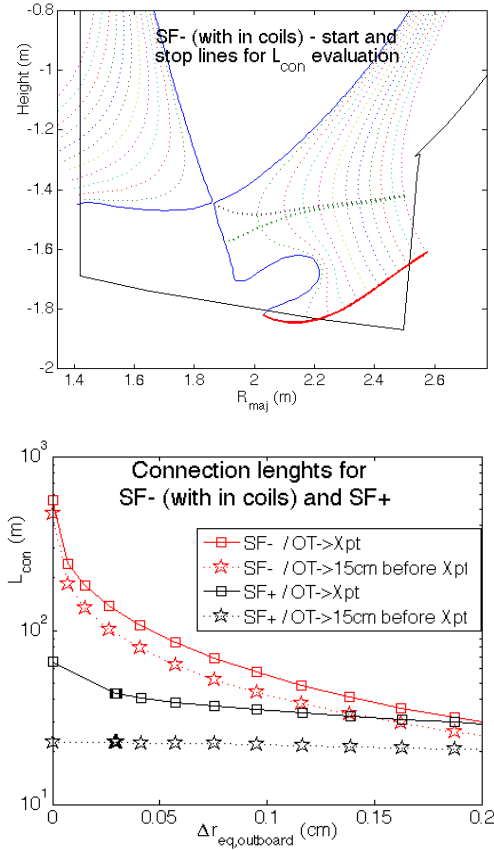


Figure 4. Top) defintion from connection length a) from x point to target; b) from half way from X point an the target; Bottom) SF⁻ Connection length evaluated for defintion a) and b) for SF⁺ and SF⁻

length is calculated from around half way between the X-point and the target up to the target. In the case of the SF⁺, for low R_L , the connection length diverges only in the case a), i.e. the main X-point feature is essentially determining the walk of the particles. On the contrary, in the case b) the connection length, for low R_L , diverges in the case b), too; this means that the second null is playing an active role and that a particle that is ionized in the region close to the plates is running a long way before impinging on the plates.

4. TECXY edge plasma simulations

The issue of the power exhaust has been analysed in this first stage with the 2D transport edge code TECXY [15]. This code allows a rather wide exploration of the operating

The results discussed for the data of Table 1 are confirmed for all flux surfaces of the SOL. At very low R_L ($R_{Flux-Surface}-R_{Boundary}$) all the alternative configurations improves (a factor between 2.5 and 5) compared to the SN, where the SF⁻ shows the higher values. Far in the SOL (large R_L) the improvements decays for all the configurations and it converges towards a factor around 1.5. A final conclusion can be worked out. Since the connection length improves in the full SOL for all the alternative magnetic configuration, a volumetric radiative improvements can be expected for all of them. The amount of expected improvements depends on which physics will play the driving part. If “classical” effect will be dominant we the X-d configuration should be the one with the larger synergy; if some non-linear effect will play a strong role we could expect a larger synergy for the configuration SF and SF⁺. The configuration SF⁻ is the most tricky one, because we could expect that both linear and non-linear effect can play an important role. The peculiarity SF⁻ is highlighted in Fig. 4, where the connection length is evaluated in two different ways for the configurations SF⁻ and SF⁺. For the case a) the connection length is calculated from the X-point up to the target; for the case b) the connection

parameter space faster than other more complex codes, as EDGED2D, SOLPS or SOLEDGE. The main reason is the simpler analytical treatment of the neutral dynamics instead of the Monte Carlo technique, while all the other main physical features are the same. The actual magnetic topology is taken into account whereas the divertor geometry is simplified with targets perpendicular to the poloidal field B_{pol} . Within the analytical model, this affects negligibly the neutrals dynamics, while maintains the ideal shape of the computing mesh close to targets, with two sides perpendicular and two parallel to B_{pol} , and so allows solving more accurately the equations. The actual fluxes can be recovered simply considering the target tilting angle. Of course these “simplifications” can affect the code “absolute” results, but when doing some parameter scan the relative results are meaningful, allowing to have a rough idea (to be confirmed by more sophisticated code) of a comparative machine performances for any plasma scenario. So far we explored only the case of pure D_2 plasma. Here we compare the standard divertor single null (SN or SD) configuration with two variants of the quasi snowflake, SF and SF^+ presented in the previous sections. As discussed before, mitigation of the target heat loads is expected for these latter. The driving mechanisms are the flux expansion, which spreads the incoming flux onto a larger area, and the enhanced volumetric losses, due to the much longer connection lengths (L_{con}), as shown in the previous section, and hence to the longer particle dwell time.

A scan on the $n_{e,s}$ value, separatrix density at the stagnation point, has been carried out between about $0.5 \leq n_{e,s} \leq 1.3 \times 10^{20} \text{ m}^{-3}$ for three values of the upstream e-folding decay length of the power flow of the SN reference case, $\lambda_{q||,u,s} = 2, 3, 4 \text{ mm}$ (see Fig. 5). These values span across that given by the empirical scaling laws [16] for DTT, namely $\geq 2.5 \text{ mm}$. The scan is repeated for $P_{\text{SOL}} = 35$ (maximum foreseen) and 25 MW, respectively with $P_{\text{SOL}}/R \approx 16$ and 12 MW/m. Since the divertor shape is still undefined, in all cases the vacuum vessel is taken as target. Consequently only a relative comparison of the loads is significant at this stage. Fig. 5 depicts the situation of the main global quantity, i.e. the fraction of the total volume power loss, plotting it versus $n_{e,s}$ for the three mentioned values of $\lambda_{q||,u,s}$, with $P_{\text{SOL}} = 35$ and 25 MW on the left and right column respectively. Losses are larger for $P_{\text{SOL}} = 25 \text{ MW}$, due to the on

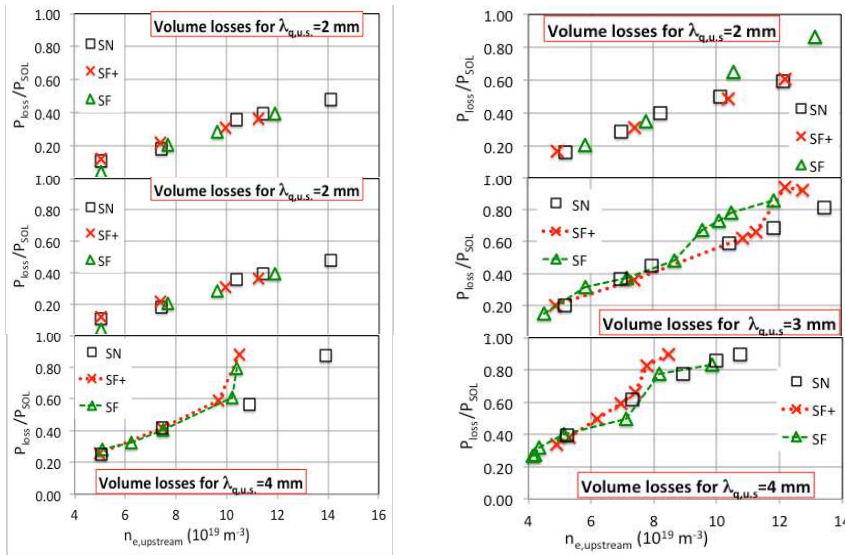


Figure 5. - Total volume power losses versus the upstream separatrix density for three different $\lambda_{q||,u,s} = 2, 3, 4 \text{ mm}$, and two different $P_{\text{SOL}} = 35 \text{ MW}$ (left column) and $= 25 \text{ MW}$ (right column).

such state is attainable for the DTT operating density range if $P_{\text{SOL}} \leq 25 \text{ MW}$. Furthermore for a given average core density SFs, should have higher $n_{e,s}$ than SN, because of the longer L_{con} ,

average lower temperatures.

Running along the columns it is seen that a sudden losses rise for both SFs can occur at enough high values of $n_{e,s}$ and $\lambda_{q||,u,s}$, except the cases $\lambda_{q||,u,s} = 2 \text{ mm}$, and $\lambda_{q||,u,s} = 3 \text{ mm}$ for $P_{\text{SOL}} = 35 \text{ MW}$. This sign of conditions very close to detachment at least, occurs earlier in density as P_{SOL} is lowered or $\lambda_{q||,u,s}$ increased. For the case with $\lambda_{q||,u,s} = 3 \text{ mm}$, the usual reference value,

as suggested by the FTU data [17] and by the present simulations, which need less particle flux entering the SOL for the same $n_{e,sep}$. The overall possible mitigation is presented in Fig. 6, as the ratio of the load peak value to the lowest density SN case of the case with $P_{SOL}=25$ MW and $\lambda_{q||,u.s}=3$ mm. This case best illustrates the effects of the advanced configurations and of the detachment, which shows as a sudden drop of the ratio. The inner target (IT) is in the upper frame, the outer target (OT) in the bottom one. The level for a sustainable load of 15 MW/m^2 is also plotted for reference as a horizontal grey line. This is, however, an upper limit to the actual load since here the targets are set perpendicular to B_{pol} . The mitigation with SF+ is always much larger on the OT than on the IT, as a result of the wider flux expansion and of the fact that the longer connection lengths shift the stagnation point towards the OT and then the total power conveyed to the IT increases, which then becomes the most critical of the two for a sustainable load. The opposite is true for SF, for which the most critical target remains the outer one. Neglecting the effect of the plate tilting, safe operation without impurities appears hard for SN (because of the OT), marginal for SF+ (because of the IT) and attainable for SF. For $P_{SOL}=35$ MW the load sustainability on both targets is hard for all configurations it is achieved only on OT for SF+ and on the IT for SF.

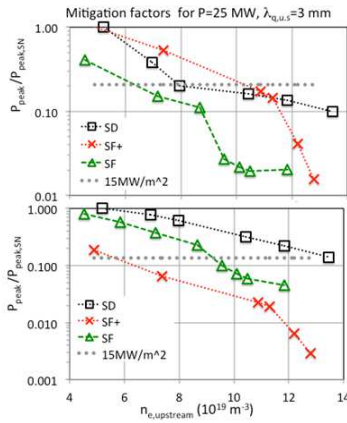


Figure 6. Mitigation factor versus the upstream separatrix density for $\lambda_{q||,u.s}=3$ mm, and $P_{SOL}=25$ MW.

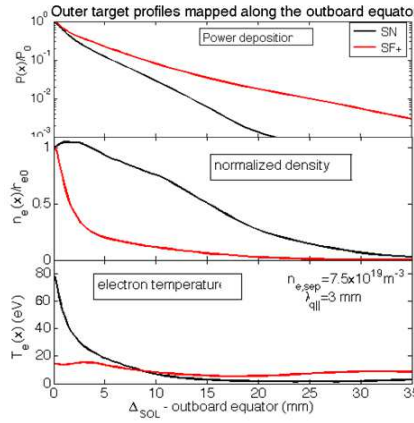


Figure 7. Various profiles on the outer target versus the outboard equatorial distance

The reason of the large load drop in the SFs are not only due to the flux expansion, but in large part also to the fact that the large increase L_{con} causes power flowing channel to widen also in terms of flux coordinates. This is evidenced for SF+ in Fig. 7, where the profiles on the OT of the power deposition and density, normalized to their peak value, and of the temperature are plotted

versus the outer equator SOL depth, in order to get rid of flux expansion effect. A well attached case with the same volume power loss is considered, namely with $P_{SOL}=35$ MW and $n_{e,s} \approx 7.5 \times 10^{19} \text{ m}^{-3}$. The SF+ channel is much wider than SN. Clearly the spreading of the power profile is due to the temperature spreading. Density adjusts its value in order to keep the pressure balance along the flux line. The main reason for this large T_e radial broadening is at present believed being caused by a significant variation occurring in the conductive parallel transport. Indeed according to the simple two point model [18], the increase of the connection length introduces changes in the upstream and target temperatures. The possible decrease of the target temperature and also of the average value along the flux tube can drop significantly the parallel conductivity. In addition, the longer length can also decrease the parallel T_e gradient along the real flux tube that further slows down the energy transport. Consequently the flow channel width must expand to ensure the same total transport rate. Experimentally a quite similar effect has been observed in ASDEX [19]. The main outcome of this study is that little difference exists between the basic SFs and SN for low working densities in term of global parameters, since the magnetic topology is modified in regions where the dissipative processes are rather negligible. At higher density instead the SFs seem susceptible of detached

operations and strongly radiating regimes, easier for lower P_{SOL} and faster cross-field diffusion. This latter may be also directly induced by the increased connection lengths.

5. Conclusions

The main objective of the Divertor Tokamak Test (DTT) facility is to host integrated experiments addressed to the solution of the power exhaust issues in view of DEMO. The installation of a set of in-vessel PF coils with currents $\leq 60\text{kA}$ enables a large variety of alternative magnetic divertor geometries. A series of potential heat flux mitigation effects have been identified for the different magnetic topologies. However, it comes clearly out that for any future reactor a strong synergy between the magnetic topology and the radiative losses will be mandatory. The machine flexibility will try to experimentally verify which is the most important physics involved for any configuration and, eventually, to understand which configuration will be more suitable for a fusion reactor. First exploration of the DTT divertor SOL indicates as very promising for the control of the power loads those configurations where the magnetic connection lengths are significantly lengthened with respect to SN. Further optimization and modelling in order to attain this goal on both divertor legs and with a high degree of reliability is in progress.

Acknowledgements

This work has been carried out within the framework of the EUROfusion Consortium and has received funding from the Euratom research and training programme 2014-2018 under grant agreement No 633053. The views and opinions expressed herein do not necessarily reflect those of the European Commission.

References

- [1] Fusion Electricity – A roadmap to the realisation of fusion energy, November 2012 (http://users.euro-fusion.org/iterphysics/wiki/images/9/9b/EFDA_Fusion_Roadmap_2M8JBG_v1_0.pdf)
- [2] R. Albanese and H. Reimerdes, "The DTT Device: role and objectives". Submitted to Special Issue of Fusion Engineering and Design entitled "DTT: Divertor Tokamak Test facility" to be published in early 2017
- [3] F. Crisanti et al., "The DTT device: choice of parameters", submitted to Special Issue of Fusion Engineering and Design entitled "DTT: Divertor Tokamak Test facility" to be published in early 2017
- [4] Allen S. et al 2012 Proc. 24th Int. Conf. on Fusion Energy (San Diego, CA, 8–13 October 2012) www-naweb.iaea.org/napc/physics/FEC/FEC2012/html/fec12.htm
- [5] G. Calabrò et al., Nuclear Fusion, 55 (2015) 083005
- [6] Soukhanovskii V.A., et al., 2011 J. Nucl. Mater. 415 S365–8
- [7] Piras F., et al., 2009 Plasma Phys. Control. Fusion 51 055009
- [8] Morris W et al 2014 IEEE Trans. Plasma Sci. 42 402
- [9] Ryutov D.D. 2007 Phys. Plasmas 14 064502
- [10] Ryutov D.D., et al., 2008 Phys. Plasmas 15 092501
- [11] R. Ambrosino, et al., to be presented at 29th Symposium on Fusion Technology (SOFT), Prague, 5th – 9th September 2016
- [12] M. Ryutov and V.A. Soukhanovskii, Phys. Plasmas 22 (2015) 110901
- [13] M. Kotschenreuther, et al., Phys. Plasmas 20 (2013) 102507
- [14] V. Pericoli Ridolfini, R. Zagórski et al. "Power exhaust evaluation for different divertor magnetic topologies of the projected tokamak DTT", poster P.2.120, presented at PSI 2016, Rome
- [15] R. Zagórski, et al., Physica Scripta. V. 70, 173–186, 2004
- [16] T. Eich et al., Phys. Rev. Lett. 107 (2011) 215001 and Nucl. Fus., 53 093031 (2013)
- [17] M. Leigh, V. Pericoli Ridolfini, R. Zagórski, Journ. Nucl. Mat., V. 241-243 (1997), p. 914-918
- [18] P.C Stangeby, "The Plasma Boundary of Magnetic Fusion Devices", Sect. 5.2, p. 221, IoP (2000).
- [19] A. Scarabosio et al, J. Nucl. Mater 463 (2015) 49